sustainability

MDPI

Article

Urban Morphology Influencing the Urban Heat Island in the High-Density City of Xi'an Based on the Local Climate Zone

Chongqing Wang, He Zhang, Zhongxu Ma, Huan Yang * and Wenxiao Jia

College of Landscape Architecture and Art, Northwest Agriculture and Forest University, Xianyang 712100, China; wcq392303@nwafu.edu.cn (C.W.); hezhang@nwafu.edu.cn (H.Z.); mazhongxu@nwafu.edu.cn (Z.M.); wxjia@nwafu.edu.cn (W.J.)

* Correspondence: yanghuan@nwafu.edu.cn

Abstract: Urban form plays a critical role in enhancing urban climate resilience amidst the challenges of escalating global climate change and recurrent high-temperature heatwaves. Therefore, it is crucial to study the correlation between urban spatial form factors and land surface temperature (LST). This study utilized Landsat 8 remote sensing data to estimate LST. Random forest nonlinear analysis was employed to investigate the interaction between the urban heat island (UHI) and six urban morphological factors: building density (BD), floor area ratio (FAR), building height (BH), fractional vegetation coverage (FVC), sky view factor (SVF), and impervious surface fraction (ISF), within the framework of local climate zones (LCZs). Key findings revealed that Xi'an exhibited a significant urban heat island effect, with over 10% of the study area experiencing temperatures exceeding 40 °C. Notably, the average LST of building-class LCZs (1-6) was 3.5 °C higher than that of land cover-class LCZs (A-C). Specifically, compact LCZs (1-3) had an average LST 3.02 °C higher than open LCZs (4-6). FVC contributed the most to the variation in LST, while FAR contributed the least. ISF and BD were found to have a positive impact on LST, while FVC and BH had a negative influence. Moreover, SVF was observed to positively influence LST in the compact classes (LCZ2-3) and open low-rise class (LCZ6). In the open mid-rise class (LCZ5), SVF and LST showed a U-shaped relationship. There is an inverted U-shaped relationship between FAR and LST, with the inflection point occurring at 1.5. The results of nonlinear analysis were beneficial in illustrating the complex relationships between LST and its driving factors. The study's results highlight the effectiveness of utilizing LCZ as a detailed approach to explore the relationship between urban morphology and urban heat islands. Recommendations for enhancing urban climate resilience include strategies such as increasing vegetation coverage, regulating building heights, organizing buildings in compact LCZs in an "L" or "I" shape, and adopting an "O" or "C" configuration for buildings in open LCZs to aid planners in developing sustainable urban environments.

Keywords: spectral indexes; land surface temperature; urban heat island; local climate zone; downscaling; thermal environment network

Citation: Wang, C.; Zhang, H.; Ma, Z.; Yang, H.; Jia, W. Urban Morphology Influencing the Urban Heat Island in the High-Density City of Xi'an Based on the Local Climate Zone. *Sustainability* **2024**, *16*, 3946. https://doi.org/10.3390/su16103946

Academic Editor: Magnus Moglia

Received: 20 February 2024
Revised: 28 April 2024
Accepted: 4 May 2024
Published: 8 May 2024

1. Introduction

Urbanization in China has surged rapidly, with 65.22% of the population residing in urban areas as of 2022 (National Bureau of Statistics of China, 2023). The rapid urbanization in China has indeed brought about significant changes in urban forms, especially in terms of the increasing use of impervious surfaces like asphalt, roofs, and concrete. These shifts have influenced cities' three-dimensional spatial structure, disrupting the urban energy balance [1] and exacerbating heat production, absorption, and retention, thereby contributing to the urban heat island (UHI) effect. The UHI effect, characterized by higher urban than suburban temperatures, presents adverse implications for inhabitants' health [2,3], energy consumption, economic activities, and environmental quality [4].

Researchers from around the world have been focusing more attention on studying and understanding the UHI effect in recent years. In current research on the UHI effect, two

main methods are commonly used for its characterization: air temperature and land surface temperature (LST). Nasehi Saeedeh et al. [5] employed LST data to characterize the UHI effect. LST data are preferred for their higher spatial resolution and their close relationship with the built environment, making LST a valuable indicator to study the impact of the UHI effect on urban climates. When it comes to retrieving LST, various algorithms such as the mono-window algorithm [6], the radiative transfer equation (RTE) method [7], and the split-window algorithm [8] are commonly used. Among these, the RTE is favored for its reliability and the fewer parameters required for Landsat 8 imagery [9]. Consequently, we opt for the RTE for LST retrieval in this study.

Urban expansion, characterized by increased impermeable surfaces and higher building density, exacerbates the UHI effect [10]. The intensity of the UHI effect is influenced by meteorological factors like relative humidity, solar radiation, and wind velocity, as well as urban morphology factors, which include building structure, land cover type, etc. [11]. The urban morphology factors include six major aspects: urban tissue configuration, street network, building-plot characteristics, land use, natural features, and urban growth. Urban morphology plays a crucial role in driving the UHI effect, as various studies have highlighted. For instance, Guo G [12] emphasized the significant contribution of urban morphology to the UHI effect, while Dirksen's study [13] revealed a strong correlation between the urban sky view factor and UHI. Studies by Muhammad [10] and Qi Yansu [14] emphasized the impact of building density and vegetation coverage on aggravating or mitigating the UHI effect, respectively. Studying the impact of multiple factors on the urban heat island effect is advantageous for gaining a deeper understanding of the urban heat island phenomenon and its driving factors. Therefore, we focus on major urban spatial morphology factors (BD, BH, FVC, ISF, SVF, FAR) frequently referenced in earlier works and proven to correlate with LST [15].

Previous research on the UHI effect has typically viewed urban areas through a simplistic "urban–suburban" lens, overlooking the intricate three-dimensional urban morphology and surface cover diversity within urban regions. This binary urban–rural perspective has limited the comprehensive exploration of UHI mechanisms across different regions within cities [16]. In response to these limitations, scholars like Stewart and Oke [17] have introduced a local climate zone (LCZ) classification system that takes into account the detailed urban internal three-dimensional morphology and surface cover variations. This new framework provides a more nuanced approach to UHI research by considering various surface parameters such as floor area ratio, sky view factor, height of roughness elements, and anthropogenic heat flux. The LCZ classification system categorizes cities into 10 types of built-up areas (LCZ1-10) and 7 types of natural cover spaces (LCZA-G) [18], with each LCZ having specific ranges for each parameter. This classification system enables the representation of different types of urban areas, allowing for a more detailed understanding of urban morphology and its relationship to the UHI effect. By considering the differences in the correlation between urban morphological factors and the UHI effect across different LCZs, insights gained from this classification system can inform urban planning strategies tailored to specific cities and zones within the same city.

Currently, research on LCZs and the UHI effect primarily revolves around two key dimensions. Firstly, within the framework of LCZs, scholars investigate the spatial and temporal heterogeneity of UHI patterns. Secondly, across diverse LCZs, the exploration delves into understanding the correlation between the UHI and its driving factors. However, current research mostly focuses on the first dimension, for instance, Zhao et al. [19] examined the variation in urban heat island intensity (UHII) within different LCZs in Shenyang City. Expanding on this, Xu et al. [20] simulated the distribution of urban heat islands in Beijing based on the LCZ zoning system. However, while the research results obtained from the second dimension often provide more effective strategies for urban sustainable development, there are currently gaps in related research. Wang et al. [21] investigated the primary factors influencing LST in various LCZs and building types in Tokyo and Shanghai. Their research discerned differences in the main factors impacting LST across different

LCZs. Overall, these studies underscore the importance of considering urban morphology, land cover composition, and spatial morphology factors in understanding the variations in LST and the UHI effect across different LCZs. Further research is needed to explore the combined impact mechanisms of multiple spatial morphology factors on LST in diverse urban environments.

In numerous previous studies, various methods such as Pearson correlation analysis [22], stepwise multiple linear regression, ordinary least square (OLS) regression [23], and geographically weighted regression [24] have been extensively used to investigate the relationship between urban spatial morphology and the urban heat island effect. However, the complex nonlinear effects of urban morphology on local temperature variations have not been fully explored. Random forest, as an ensemble of tree predictors, relies on the values of independently sampled random vectors for each tree. The generalization error of random forest converges as the number of trees in the forest increases [25]. In contrast, random forest can better handle the complex and variable nonlinear relationships between urban spatial morphology and the urban heat island effect. For example, Ming Y. et al. [26] used the random forest model with data from 162 prefecture-level cities in China to reveal the nonlinear effects of urban morphology and industrial morphology on diurnal and nocturnal surface urban heat islands (SUHIs) and their contributions to the variance of diurnal and nocturnal SUHIs. Similarly, Gao Y. et al. [27] conducted a comprehensive assessment of the thermal environment in five representative blocks in Xi'an, China, using the random forest model to explore the nonlinear relationship between urban spatial characteristics and local thermal environments and to rank their contributions.

The study focusing on Xi'an, known as one of the ten furnace cities in China, aims to delve into the UHI effect within the city with a comprehensive approach. Firstly, the study analyzed UHII through LST retrieval using Landsat 8. Secondly, Landsat 8 imagery and OpenStreetMap data were used to evaluate urban morphological factors (BD, FAR, BH, FVC, SVF, ISF) and map LCZs of the study areas in Xi'an. Then, the study explored the correlation between LST and urban morphology factors using random forest nonlinear analysis for each LCZ. This study aims to explore the nonlinear correlation between LST and urban spatial morphological factors in different LCZs, providing strategic insights for mitigating the UHI effect in various urban forms in Xi'an. Ultimately, this research seeks to facilitate more resilient and sustainable urban development practices.

2. Materials and Methods

2.1. Study Area

Xi'an, a major city in western China, serves as the core city in the Guanzhong Urban Cluster (Figure 1). Known as one of the ten furnace cities in China, Xi'an has a significant UHI effect. Previous studies, such as the study by Gao et al., have highlighted the intensification of high temperatures in Xi'an over the years. For instance, there was an increase in the average temperature from 32.34 °C in 2000 to 42.45 °C in 2016. Additionally, the high-temperature area expanded from 40.59 square kilometers in 2000 to 81.52 square kilometers in 2016, marking a growth of 100.87%. The study area in this paper was four central districts of Xi'an, namely, Xincheng District, Yanta District, Lianhu District, and Beilin District. These four districts were the inner city of Xi'an, with the highest urbanization level and highest population density. It is a typical sample for analyzing the relationship between the UHI and urban morphology factors through an LCZ approach.

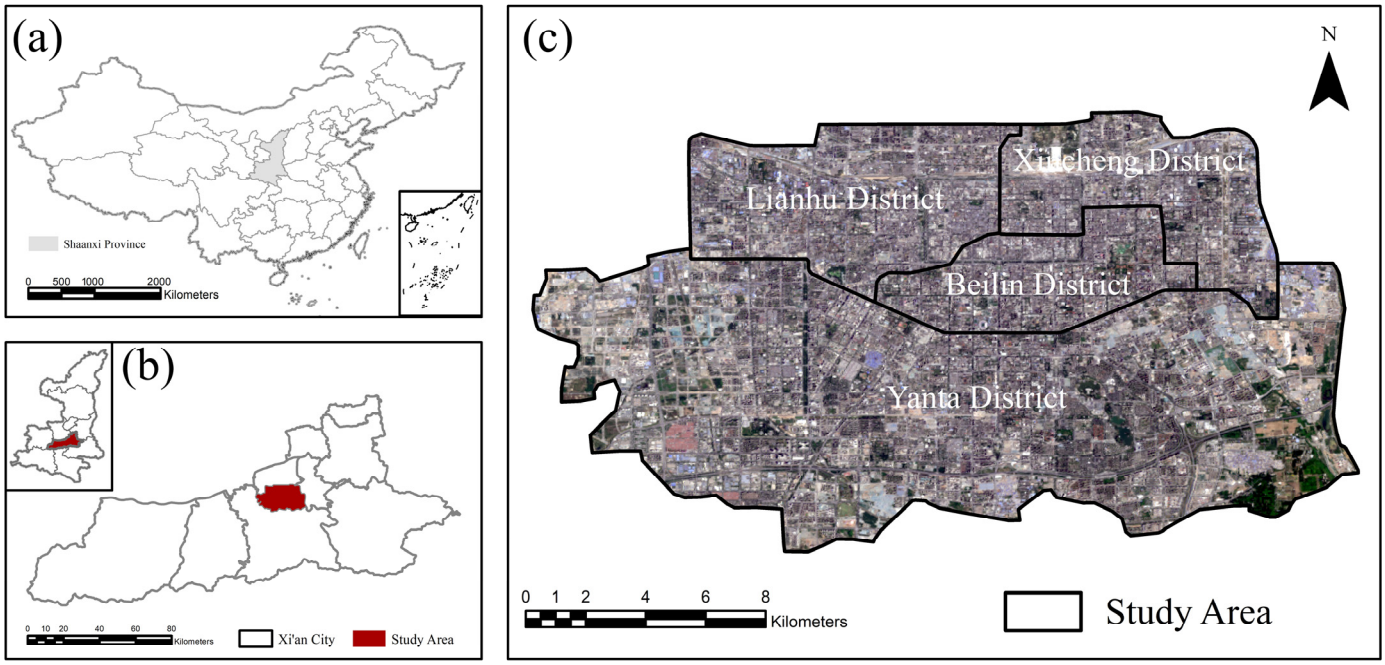

Figure 1. Location of the study area: (**a**) Shaanxi province; (**b**) Xi'an City; (**c**) study area.

2.2. Date Sources

This study utilized Landsat 8 remote sensing image data (captured on 30 June 2021, at 3:19 A.M., and 2 August 2021, at 03:19 A.M.), building footprint outline data (dated 2021), and building height data (dated 2021). Table 1 contains detailed information on the specific sources used.

Table 1. Data type and description.

Date	Use	Date Sources	Date Types
Landsat 8 remote sensing image data	Used to retrieve land surface temperature, calculate fractional vegetation coverage, and extract impervious surface	https://earthexplorer.usgs.gov/ (accessed on 1 October 2023)	Raster data with a 30 m resolution
Building footprint outline data	Used to calculate building density, floor area ratio, and sky view factor	https://www.openstreetmap.org/ (accessed on 1 October 2023)	Vector data
Building height data	Used to calculate average building height, floor area ratio, and sky view factor		

2.3. Land Surface Temperature Retrieval

In this study, the land surface temperature inversion principle, utilizing the radiation equation method [28,29], involves subtracting atmospheric thermal radiation from the total sensor-obtained thermal radiation. This process derives the thermal radiant intensity emitted by the land surface, enabling subsequent calculation of the land surface temperature. The thermal radiant intensity (L_λ) obtained by the sensor is calculated as follows:

$$L_\lambda = [\varepsilon \times B(T_S) + (1 - \varepsilon)L\downarrow] \times \tau + L\uparrow \quad (1)$$

where:

- ε—Surface radiance, calculated using the NDVI threshold method;
- T_S—Surface temperature expressed by thermodynamic temperature;

- $B(T_S)$—Thermal radiant intensity of the blackbody at e temperature derived from Planck's law;
- τ—Atmospheric transmittance in the thermal infrared band;
- $L\uparrow$ / $L\downarrow$—The upward/downward radiance of the atmosphere.

The radiant intensity $B(T_S)$ of the blackbody in the thermal infrared band is as follows:

$$B(T_S) = \frac{[L_\lambda - L\uparrow - \varepsilon \times (1-\varepsilon) L\downarrow]}{(\tau \times \varepsilon)} \quad (2)$$

L_λ can be calculated from the DN-value of the image.

$L\uparrow$, $L\downarrow$, and τ parameters can be obtained by inputting the longitude and latitude of the image center and the imaging time on the NASA official website (http://atmcorr.gsfc.nasa.gov/, accessed on 27 April 2024). $L\uparrow$ = 1.96, $L\downarrow$ = 3.20.

ε is atmospheric transmittance, and it is calculated by dividing the image into water bodies, buildings, and vegetation using a mixed pixel decomposition method. ε = 0.77.

Finally, the surface temperature is calculated according to the radiant intensity of the thermal infrared band received by the sensor and the inverse function of Planck's formula. The formula is as follows:

$$T_S = \frac{K_2}{\ln[\frac{K_1}{B(T_S)} + 1]} \quad (3)$$

For Landsat 8 satellite data's 10th band, K_1 and K_2 values are 774.89 W/(m^2 μmsr) and 1321.08 K, respectively.

Lastly, the final LST was calculated using the ArcGIS v10.8 raster calculator tool to compute the average value.

2.4. Delimitation of Local Climate Zone

A GIS-based approach was utilized to delimitate LCZs [30]. This method has been previously developed and tested in Prague and Brno, the two largest cities in the Czech Republic [31]. The approach is founded on measurable urban spatial morphology factors, inspired by the fundamental factor parameters defined by Stewart and Oke [17], and influenced by the research conducted by Yurong Shi and colleagues [32]. In this study, seven urban spatial morphology factors were chosen as the basis for LCZ zoning: BH, BD, ISF, SVF, FVC, and water ratio (WR) and FAR. The classification process involved dividing the study area into 300 m × 300 m grids, from which these physical parameters were extracted. LCZ zoning was then performed using specific thresholds. The entire process consisted of three steps: first, defining the fundamental research units; second, determining the LCZ zoning factors and conducting calculations; and finally, establishing the LCZ zoning thresholds to complete the zoning. The process diagram is presented in Figure 2.

2.4.1. Defining Grid Units

Spatial autocorrelation is a geographic phenomenon whereby entities that are closer together tend to exhibit more similarity than those that are far apart. This method can be employed to examine the relationship between data variance and spatial distance. In this study, we utilize spatial autocorrelation to identify the range within which building heights exhibit pronounced autocorrelation. This information is crucial for determining an appropriate grid size that ensures consistent building heights and minimizes errors associated with unsuitable grid sizes.

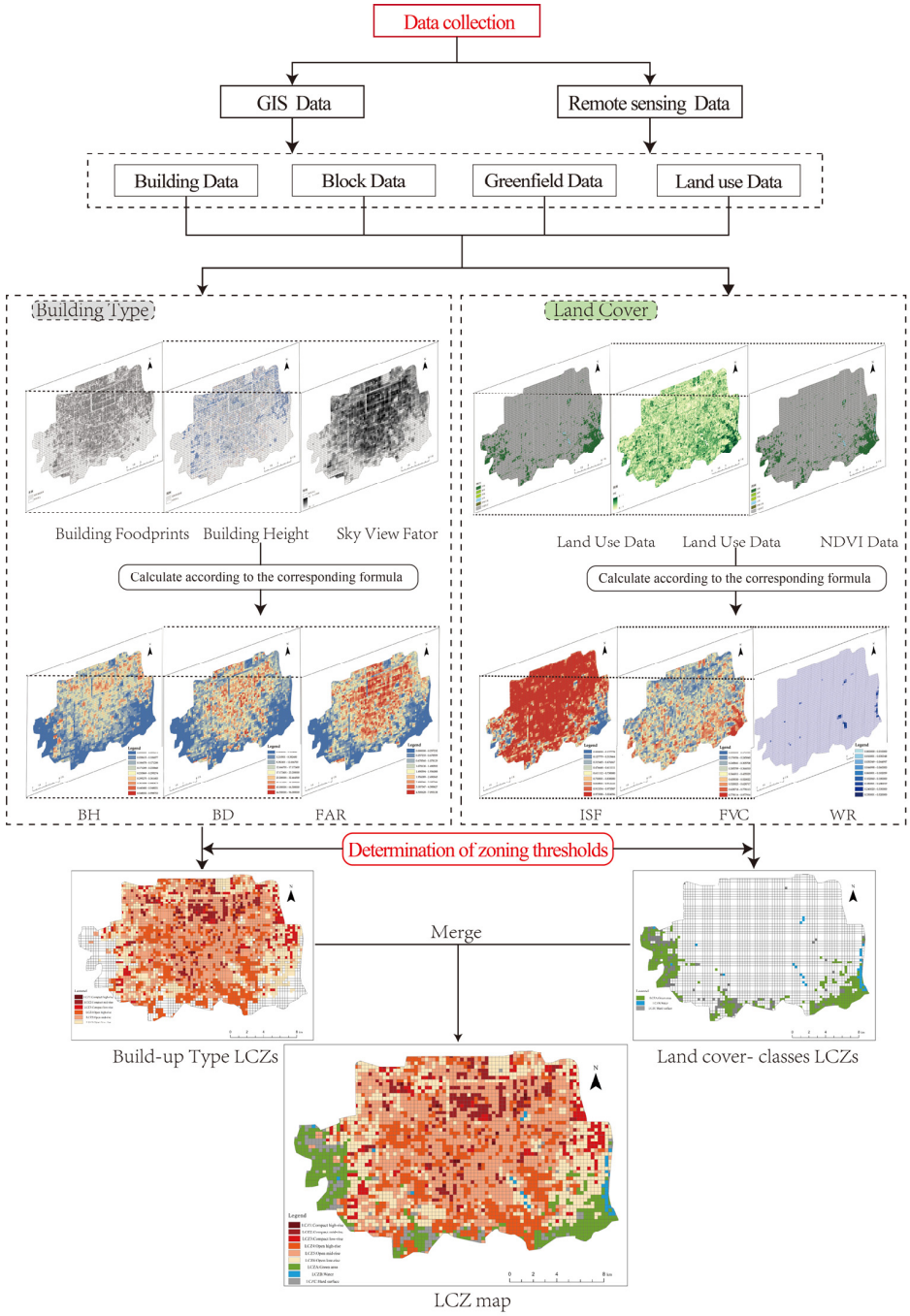

Figure 2. Schematic diagram of LCZ zoning steps.

To analyze the spatial relationship of features, we employ the spatial autocorrelation tool in ArcGIS, defining the spatial weights as INVERSE_DISTANCE. The weights assigned to building height are standardized, meaning that each weight is calculated as the sum of weights for all neighboring features. Ultimately, a distance threshold is established to identify strong autocorrelation in building heights. This threshold serves as the foundational grid size for the research units, and the resulting outcomes are evaluated based on *p*-values and z-scores to assess the confidence of the obtained results.

2.4.2. Determine Morphology Factors for Each Grid

Based on the fundamental factor parameters defined by Stewart and Oke [17], and taking into consideration the research of Yurong Shi [32], Yuan Bo [33], and others, we chose seven urban spatial morphology factors, namely, building height (BH), building

density (BD), impervious surface fraction (ISF), sky view factor (SVF), fractional vegetation coverage (FVC), water ratio (WR), and floor area ratio (FAR), as the key components for LCZ mapping. The values of these factors were calculated using ArcGIS v10.8 software. For specific formulas and additional details, please refer to Table 2.

Table 2. Definition and calculation method of the seven urban spatial morphological factors.

Spatial Morphology Factors	Definition	Calculation Method	Date Sources
BH	Average building height in the study area	$BH = \frac{\sum_{n=1}^{n} BH_i}{n}$ Where BH_i is the building height and n is the number of buildings	OpenStreetMap
BD	The ratio of the building base area to the total area of the area in the study	$BD = \frac{\sum_{i=1}^{n} BS_i}{S_{site}}$ Where BS_i is the building base area and S_{site} is the total site area of the area in the study	OpenStreetMap
FAR	The ratio of the total amount of floor area that buildings have to the total area of the area in the study	$FAR = \frac{\sum_{i=1}^{n} (BS_i \times BF_i)}{S_{site}}$,where BS_i is the building base area, BF_i is the average number of floors in buildings, and S_{site} is the total site area of the area in the study	OpenStreetMap
SVF	Used to describe the degree to which the sky in the study area is obscured by surrounding obstacles	$SVF = 1 - \frac{\sum_{i=1}^{n} \sin \gamma_i}{n}$ Where γ_i is the maximum building height angle within the sector corresponding to the azimuth angle in the study area and n is the number of calculated azimuth angle in the study area	OpenStreetMap
ISF	The ratio of the area covered by various impermeable building materials to the total area of the underlying surface in the study area	$ISF = \frac{S_i}{S_{site}}$ Where S_i is the area paved with hard materials and S_{site} is the total site area of the area in the study	Land use map in 2021
WR	The ratio of the water area to the total area of the area in the study	$WR = \frac{\sum_{i=1}^{n} WS_i}{S_{site}}$ Where WS_i is the water area and S_{site} is the total site area of the area in the study	Land use map in 2021
FVC	Percentage of vertical projected area of vegetation in the study area	$FVC = \frac{NDVI - NDVI_{soil}}{NDVI_{veg} - NDVI_{soil}}$ $NDVI = \frac{NIR - RED}{NIR + RED}$ Where $NDVI_{soil}$ is the NDVI value of the pixel covered by pure bare soil and $NDVI_{veg}$ is the NDVI value of pure vegetation coverage pixels. After repeated comparisons the NDVI value with a cumulative frequency of 2% and 98% was taken to be $NDVI_{soil}$ and $NDVI_{veg}$, respectively [34]	Landsat 8-OLI remote sensing image date

2.4.3. LCZ Mapping

The original LCZ classification system divided urban areas into ten urban building classes (LCZ1-10) and seven land cover classes (LCZA-G) [17]. In this paper, LCZs are divided into six building classes (LCZ1-6) and three land cover classes (LCZA-C) according to the actual situation in Xi'an and the research of Christopher O'Malley et al. [35,36]. Small amounts of LCZ7 and LCZ9 were merged into LCZ3 and LCZ6, and small amounts of LCZ8 and LCZ10 were merged into LCZ6, respectively, and all the natural land cover (LCZA-D and LCZF in the original classification system) was grouped into one category: LCZA. We renamed LCZE and LCZG as LCZB and LCZC.

The zoning process was conducted in several steps. The primary research units were initially classified into two core classes: building classes and land cover classes, determined

by BD. Subsequently, LCZs classified under building classes were further segregated into compact and open categories based on BD, SVF, and FAR criteria. Similarly, the LCZs related to land cover classes were further divided into LCZA, LCZB, and LCZC using the fraction of FVC, WR, and ISF. The introduction of LCZ is presented in Table 3.

Table 3. Description of local climate zone types.

Local Climate Zone			Figure	Definition
Building-classes	Compact class	LCZ1 Compact high-rise	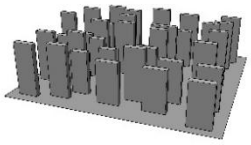	High-rise buildings (10 stories or more) are closely mixed, and trees, green spaces, etc., are scarce. The surface is mainly covered with hard paving such as concrete. A large number of building materials such as concrete, steel, stone, and glass are used
		LCZ2 Compact mid-rise	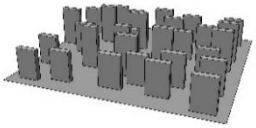	Mid-rise buildings (3–9 stories) are closely mixed, with few trees, green spaces, etc. The surface cover is mainly hard paving such as concrete. A large number of building materials such as concrete, stone, and tiles are used
		LCZ3 Compact low-rise	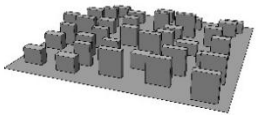	Low-rise buildings (1–3 stories) are closely mixed, with few trees, green spaces, etc. The surface cover is mainly hard paving such as concrete. A large number of building materials such as concrete, stone, and tiles are used
	Open class	LCZ4 Open high-rise		High-rise buildings (10 stories or more) are open and scattered, with abundant permeable underwater surfaces (low plants, sparse trees), and building materials are mainly concrete, steel, stone, glass, etc.
		LCZ5 Open mid-rise		Mid-rise buildings (3–9 stories) are open and scattered, with abundant permeable underwater cushions (low plants, sparse trees), and the building materials are mainly concrete, steel, stone, glass, etc.
		LCZ6 Open low-rise		Low-rise buildings (1–3 stories) are open and scattered, with abundant permeable underwater surfaces (low plants, sparse trees), and building materials are mainly concrete, stone, wood, etc.
Land cover-classes		LCZA Green area	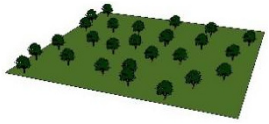	A landscape with a large number of vegetation or herbaceous plants, and the area is often divided into natural grasslands, agriculture, or natural parks
		LCZB Water area	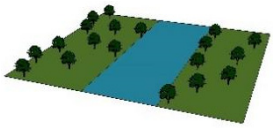	Lakes, seas, and other large areas of water landscape, or small areas of rivers, reservoirs, reservoirs, etc.
		LCZC Hard surface area	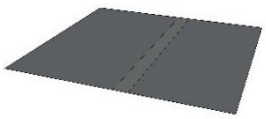	The surface cover is mainly stone or paved, basically no vegetation cover, and the area is often desert or urban roads

2.5. Data Analysis and Modelling

For the investigation of the nonlinear relationship between LST and various influencing factors, this study utilized a random forest regression model. The random forest regression model, proposed by Breiman [25], is a nonlinear machine learning approach and an enhancement of decision trees. In this study, the random forest model was employed to characterize the importance of each factor on LST. Additionally, partial dependence plots were used to reveal the nonlinear and complex relationships between each factor and LST. During the construction of the random forest model, two important parameters were considered: the number of trees (ntrees) and the number of variables used for splitting at each tree node (mtry). Through testing, ntrees was set to 500, as it yielded the lowest root mean square error (RMSE%) and highest model accuracy. mtry was set to its default value of 4. A 70% subset of the data was randomly selected as the training set, with the remaining 30% reserved for testing purposes.

3. Results

3.1. Characteristics of LST

The average LST of the study area was 37.7 °C. It was found that more than 40% of the study area experienced LST exceeding 38 °C, which indicates a significant UHI effect. Furthermore, extremely high LSTs surpassing 40 °C were observed in over 10% of the area. The highest LST recorded during the study was 50.8 °C, observed in the central part of Lianhu district, which is primarily characterized by industrial land use. Conversely, the lowest LST of 29.2 °C occurred in the southeastern part of Yanta District, which was an ecological park. Overall, the study area exhibited the characteristic of a "lower in the south and higher in the north" urban heat island effect. Specifically, the northern districts of Lianhu, Beilin, and Xin Cheng displayed higher average LST compared to the southern district of Yanta. Please refer to Figure 3 for an illustration of these LST variations.

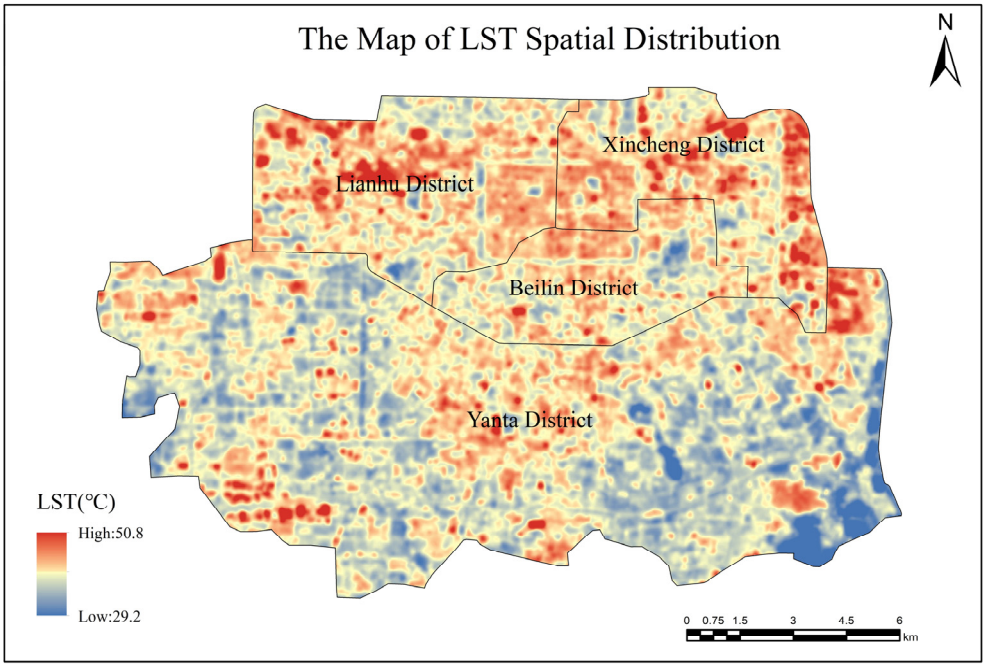

Figure 3. The LST map of the study area.

3.2. LCZ Map

Spatial autocorrelation analysis indicated a stable correlation at a building height of 269.83 m, supported by a z-score of 415, with a probability of less than 1% for the clustering pattern to occur randomly (p-value = 0). As a result, the study adopted a basic research unit size of 300 m × 300 m. In each grid, the six morphology factors were extracted and

calculated. The thresholds for each LCZ type were ultimately determined by the results of six urban morphology factors and previous research by Stewart [17], Yurong Shi [32], Yuan Bo [33], and others, as shown in Table 4.

Table 4. Local climate zone zoning thresholds.

Local Climate Zone		BD	BH	SVF	ISF	FVC	FAR	WR
Building classes	LCZ1	0.4–0.8	27–36 m	0.5–0.8	0.8–1	0.1–0.3	2–5	<0.1
	LCZ2	0.4–0.8	9–27 m	0.6–0.9	0.8–1	0–0.6	1–4	<0.1
	LCZ3	0.4–0.8	0–9 m	0.7–1.0	0.5–0.8	0–0.5	0–2	<0.1
	LCZ4	0–0.4	27–36 m	0.5–0.9	0.2–1	0.1–0.7	0–6	<0.1
	LCZ5	0–0.4	9–27 m	0.6–1.0	0.2–1	0.1–0.8	0–4	<0.1
	LCZ6	0–0.4	0–9 m	0.7–1.0	0–1	0.1–0.9	0–2	0–0.4
Land cover classes	LCZA	<0.1	0 m	>0.9	0–0.5	0.1–1	<0.1	<0.1
	LCZB	<0.1	0–6 m	>0.9	0.0.5	0.1–0.7	<0.1	0–0.6
	LCZC	<0.1	0 m	>0.9	0.1–1	0–0.8	<0.1	<0.1

LCZ5 (open mid-rise) ranked the first, with 34.98% of the total area, occurring in the central areas of the study area (Figure 4). LCZ6 (open low-rise) followed, with proportion of 20.65%, forming a strip-like distribution along the edges of the study area. The proportion of LCZ4 (open high-rise), LCZ2 (compact mid-rise) and LCZ3 (compact low-rise) were 17.86%, 6.23%, and 4.42%, respectively. The LCZA (green area) and LCZC (hard surface area) occurred along the southern edges of the study area, whose proportions were 10.09% and 4.59%, respectively. Following the LCZB (water area) with 0.82%, LCZ1 (compact high-rise) was the least, with the proportion of 0.36% of the total area, with few and scattered occurrences.

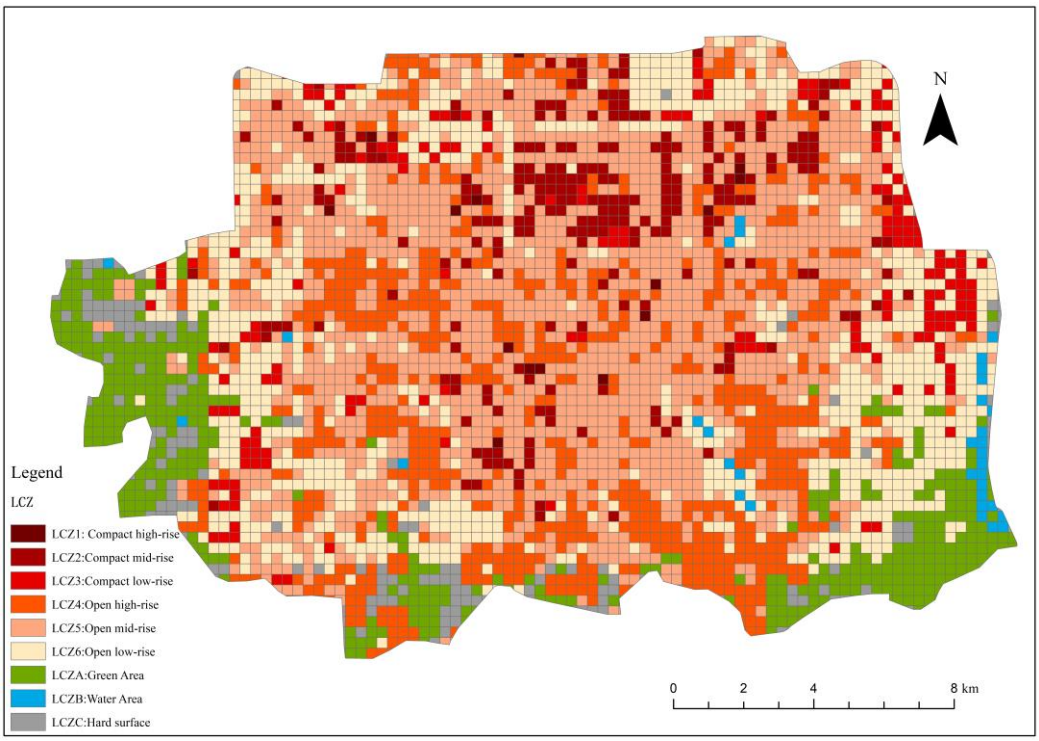

Figure 4. The LCZ map of the study area.

3.3. LST Differences in LCZs

The study area had an overall average LST of 37.7 °C, as represented by the red line in Figure 5. The average LST in building-class LCZs (1-6) was slightly higher at 39.7 °C, recording a 2 °C increase compared to the overall average LST of the study area. Conversely,

land cover-class LCZs (A-C) exhibited an average LST of 36.2 °C, which was 1.5 °C lower than the overall average LST. Notably, the average LST of building-class LCZs (1-6) was 3.5 °C higher than that of land cover-class LCZs (A-C). Among building-classes LCZs (1-6), the average LST of compact LCZs (1-3) was 2.4 °C higher than open LCZs (4-6). LCZ3 (compact high-rise) had the highest LST, reaching 40.3 °C, while LCZB (water area) had the lowest LST, as low as 33.6 °C. The overall order of the mean LST was LCZB < LCZA < LCZ4 < LCZC < LCZ6 < LCZ5 < LCZ1 < LCZ2 < LCZ3.

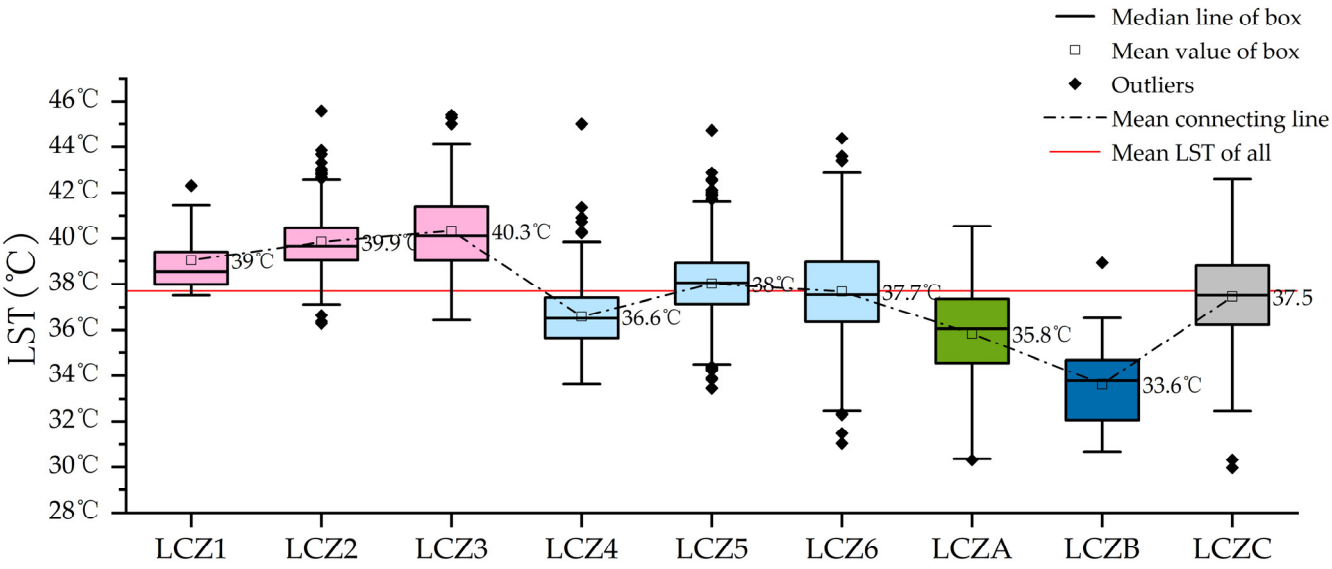

Figure 5. LST boxplot within LCZs.

3.4. Nonlinear Analysis Results of Various Influence Factors and LST

The importance of various urban spatial morphology factors on model features was presented in Figure 6. The study revealed that FVC was the most influential factor affecting LST, exhibiting the highest impact across almost all LCZs. Conversely, FAR contributed relatively less to LST variations. For land cover-class LCZs, ISF and FVC, the two natural coverage factors, were the most significant contributors to LST variations. A comparison between the importance analysis results and Pearson correlation analysis is illustrated in the Figure 6. It was observed that some factors with high Pearson correlation coefficients also obtained high-importance scores, indicating their significant influence on temperature, such as FVC, SVF, BH, and BD.

The results from random forest analysis unveiled the intricate relationships between urban spatial morphology factors and LST, surpassing the simplicity of linear correlations, and the results of partial correlation analysis were shown in Figure 7. BD demonstrated a significant warming effect between 0.2 and 0.4. BH, within the range of 0–40 m, exhibited a rapid decrease in LST with increasing BH. Between 40 and 60 m, there was minimal variation in LST with increasing building height. However, when BH exceeded 60 m, the relationship with LST became positive. FAR displayed a positive correlation with LST when FAR ranged from 0 to 1.5. Once FAR surpassed 1.5, the correlation with LST became negative. FVC demonstrated a nearly linear negative correlation with LST. ISF exhibited a positive correlation with LST. Between ISF values of 0.2 and 0.5, LST increased exponentially with increasing ISF. However, after ISF reached 0.5, the rate of increase in LST slowed down. SVF showed a positive correlation with LST in the compact class (LCZ2-3) and open low-rise class (LCZ6). In the open mid-rise class (LCZ5), SVF and LST exhibited a U-shaped relationship, with the inflection point occurring between 0.75 and 0.85.

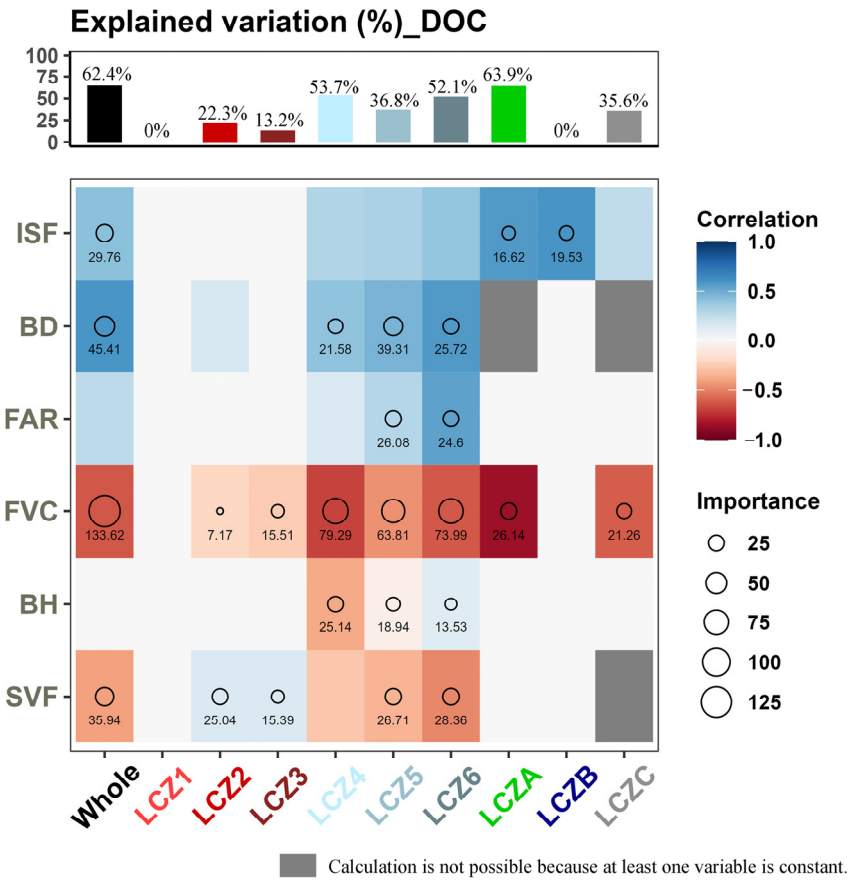

Figure 6. The contribution of each spatial morphology factor to LST.

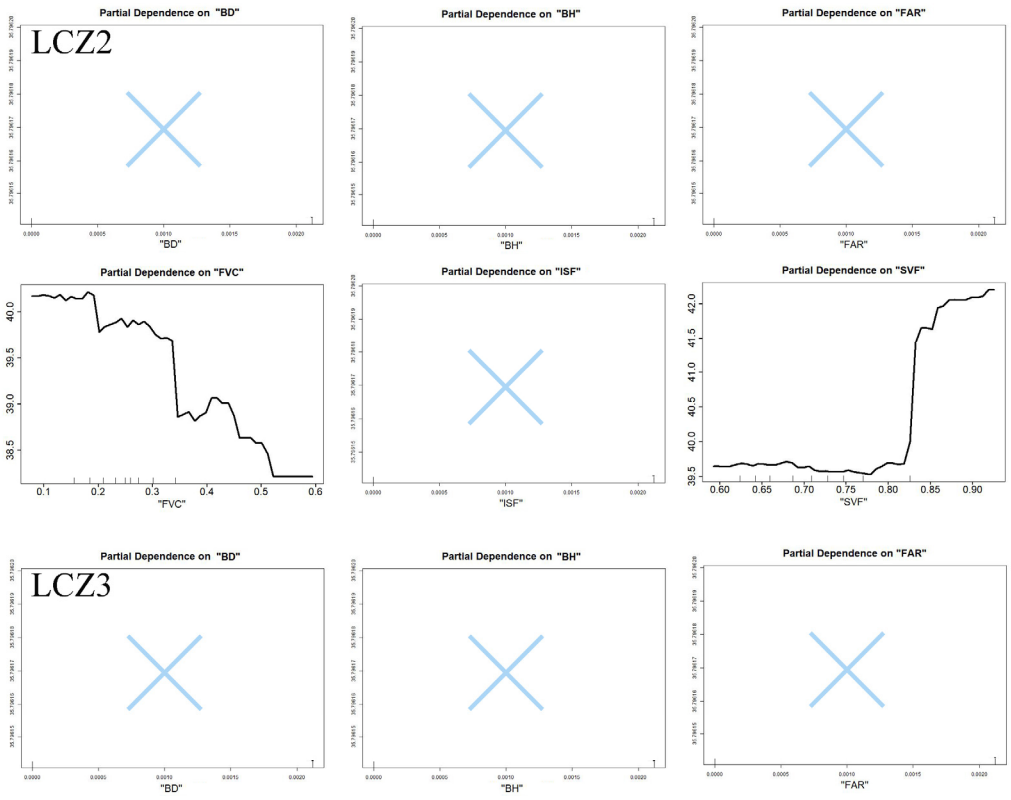

Figure 7. *Cont.*

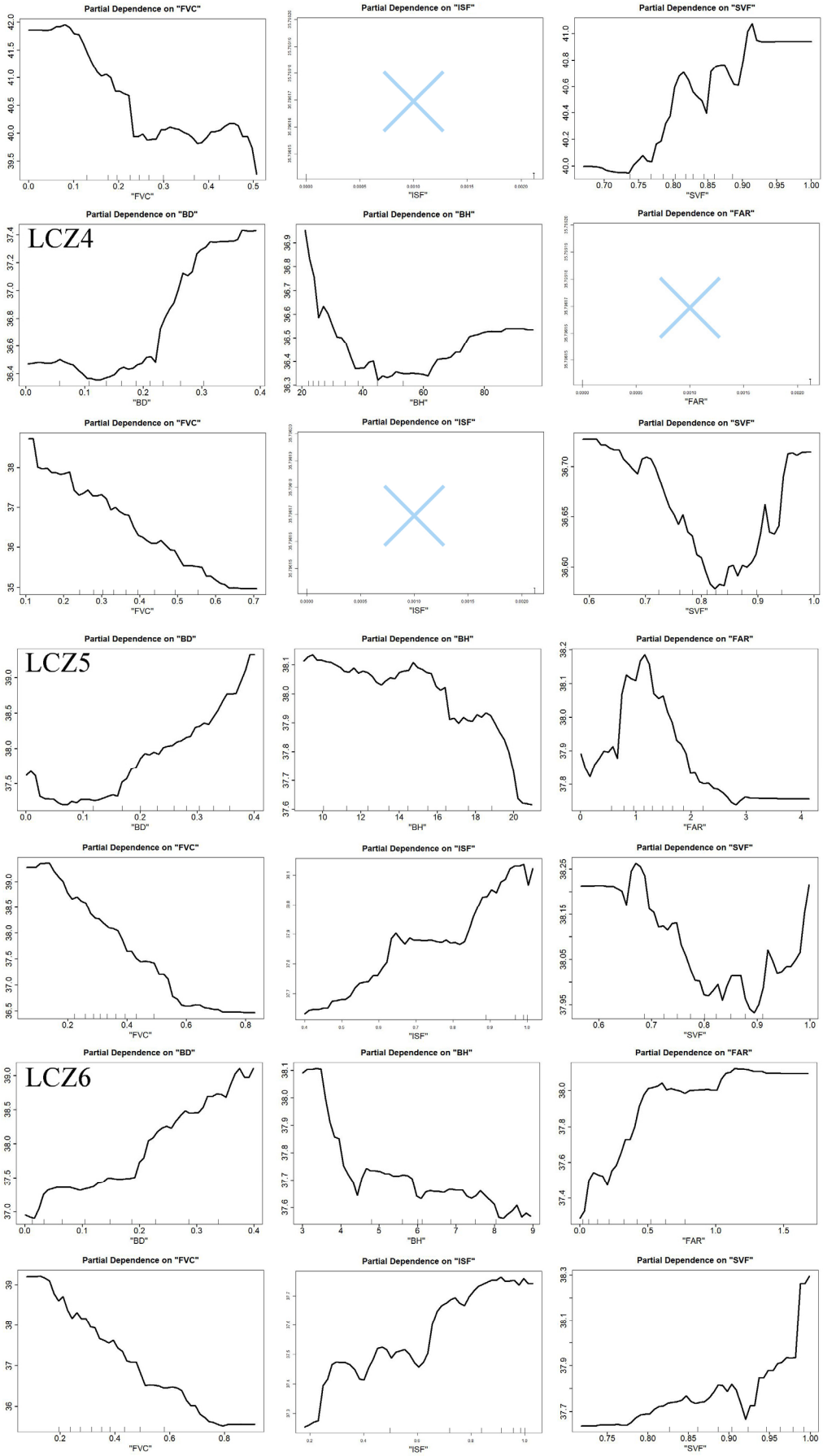

Figure 7. *Cont.*

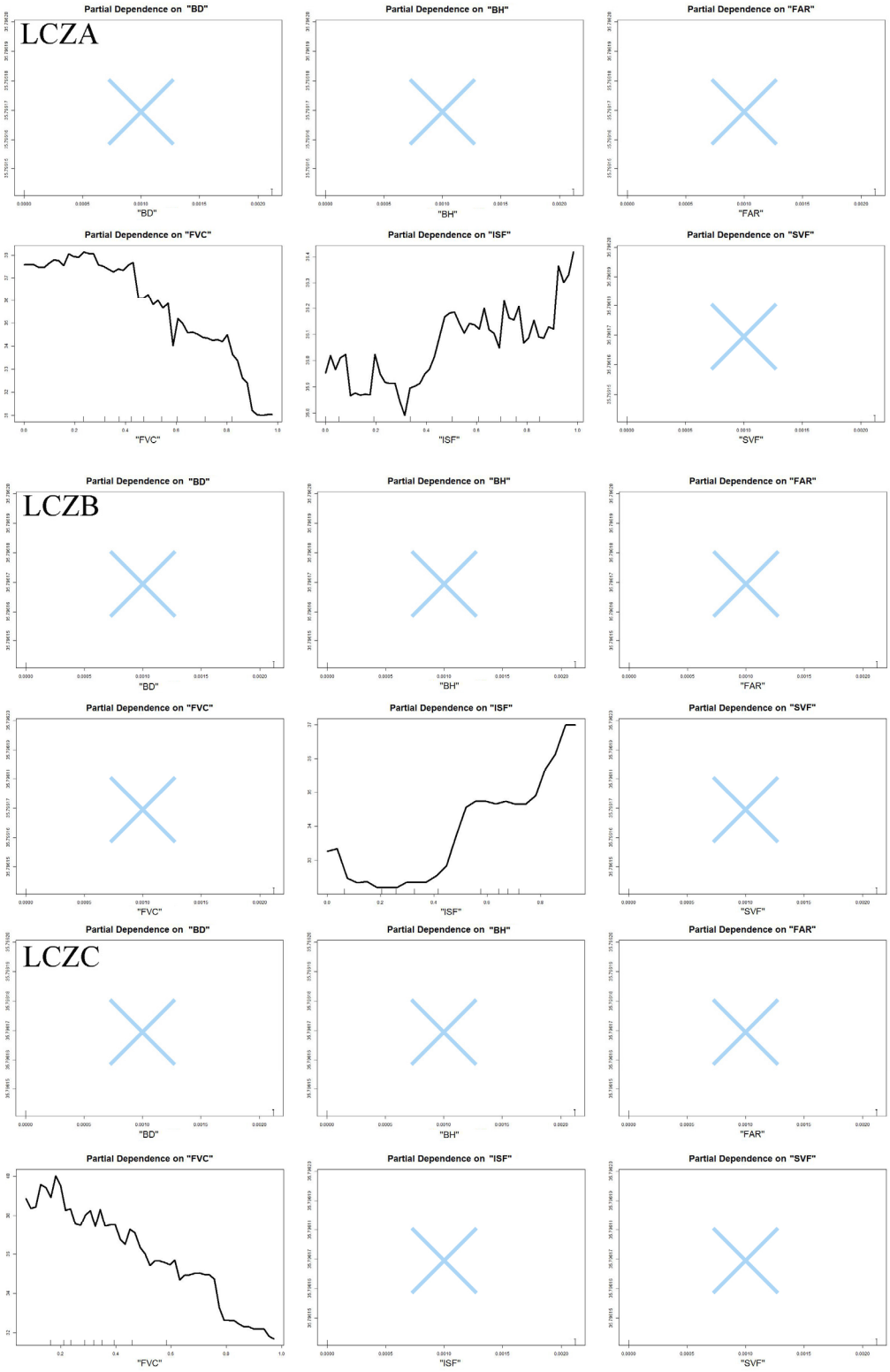

Figure 7. *Cont.*

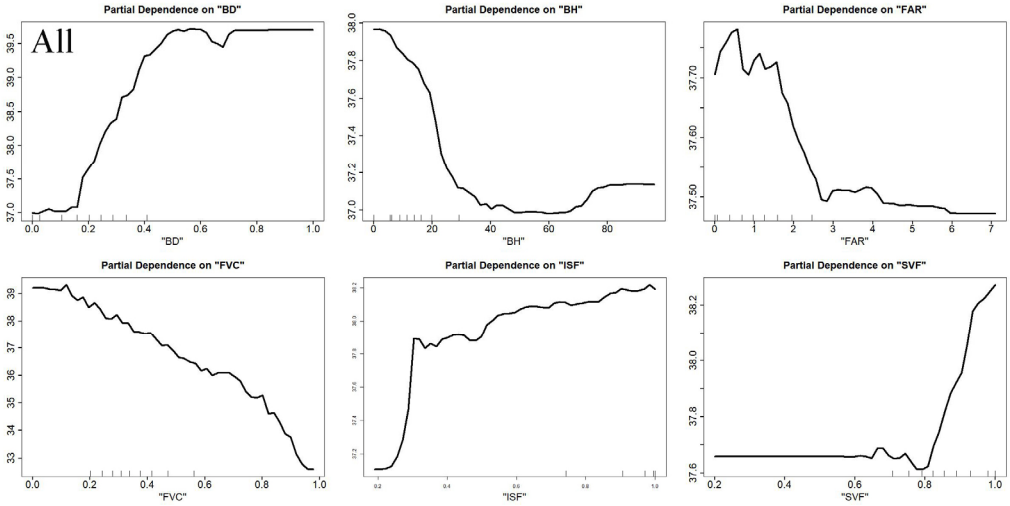

Figure 7. The results of the partial correlation analysis.

4. Discussion

4.1. The Characteristics of LST among LCZ Types

This study corroborates previous research conducted in diverse geographical settings, including Texas [37], Nanjing [38], Xi'an [39], Wuhan [40], and other locations, that building LCZ classes exhibit higher LST compared to land cover LCZ classes. This difference can be attributed to the prevalence of heat-absorbing materials, such as concrete and asphalt, in building LCZs, while land cover LCZs predominantly feature extensive pervious surfaces that help mitigate the UHI effect.

Among building LCZs, the LST of compact LCZs (LCZ1-3) was observed to be higher than that of open LCZs (LCZ4-6), aligning with earlier findings in cities such as Xi'an [41] and Nanjing [38]. This difference is likely due to compact blocks generally having a higher building surface area compared to open blocks. The combination of low solar radiation heat flux and a large heat storage capacity per unit area results in higher LSTs in high-density areas [42].

Within compact LCZs, the sequence of observed land surface temperature (LST) values was LCZ3 > LCZ2 > LCZ1, aligning with similar findings documented in Nanjing [38]. However, Cai et al. [43] reported the opposite pattern for compact LCZ types in Shanghai and Hangzhou. Meanwhile, Zhang et al. quantitatively analyzed the variation in urban land surface temperature during the land use transition process in Xi'an from 2000 to 2019, reporting that the average LST of LCZ2 types was higher than that of LCZ1 and LCZ3. These findings suggest that the order of mean LST of compact LCZs (LCZ1-3) is not a fixed rule.

Similar variability is observed in open LCZs. For instance, Yang et al. found that the order of mean LST was LCZ6 > LCZ5 > LCZ4 [44], while Liu et al. found that LCZ4 > LCZ5 = LCZ6 [45]. This variability can be attributed to the dual mechanisms of LCZ increase from heat-absorbing surface materials and temperature decrease from building shadows and local ventilation [46]. The differences in city size, local climate, and other factors can also contribute to the variability in LST patterns among open LCZs. Overall, the complex interactions among these factors contribute to the variability observed in UHI patterns.

4.2. Discussion on the Relationship between Urban Spatial Form Factors and LST Based on LCZ

FVC was negatively correlated with the LST, whereas ISF, FAR, and BD had significant positive effects. These findings were consistent with those of previous studies, such as that of Liang Zhou [47], Luciana Schwandner Ferreira [48], Zhongli Lin [49], and others.

Consistent with the findings of Liang Zhou [47], Luciana Schwandner Ferreira [48], Zhongli Lin [49], and other researchers, this study revealed a negative correlation between LST and FVC in all LCZs. This correlation could be attributed to the potential of urban vegetation to mitigate the UHI effect through shading and transpiration. Studies by Doick and Hutching [50] demonstrated that vegetation could reduce the penetration of sunlight, convert solar radiation into latent heat through photosynthesis, and thereby slow down surface warming [51]. Compared to the research findings of other scholars, our study revealed a more significant negative correlation between FVC and LST. This difference in results could be attributed to the fact that most green spaces in our study were concentrated in parks with large areas and high density, while also being relatively distant from high-density built-up areas. Supported by the findings of Baojuan Zheng [52] and Alavipanah [53], aggregated green spaces had a more pronounced cooling effect, and their distance from high-density built-up areas contributed to their enhanced cooling effects. Consequently, the negative correlation between FVC and LST was more prominent in this study.

Similar to the results of Liang Zhou's study [47], ISF and LST exhibited a positive correlation. The reason was that impermeable surfaces like concrete and asphalt replaced soil and vegetation in urban structures [54,55]. The change in land cover led to changes in the urban canopy structure and a reduction in latent heat flux, with the sensible heat flux and radiation heat flux from impermeable surfaces being significantly greater than those from natural land cover. This resulted in an increase in LST.

BD exhibited a positive correlation with LST. As BD increased, the rate of LST increase was highest between 0.2 and 0.4; beyond 0.4, the increase stabilized. This phenomenon is highly consistent with the research findings of Wang et al. [56] and Gao et al. [27]. The increase in building density affects both the impervious surface coverage and the urban wind environment in the formation of urban canyons [57]. Specifically, the formation of urban canyons leads to rapid warming of canyon walls during the day, producing a significant amount of sensible and radiation heat flux within the canyon [58]. The bottom of the canyon, due to its larger heated area, stores a significant portion of solar radiation flux and heat flux from the canyon walls. At night, the bottom of the canyon releases the heat absorbed during the day, but it is blocked by the canyon walls, resulting in the circulation of heat within the urban canyon and difficulty in releasing heat [58]. However, there is a threshold for the warming effect described above. When BD exceeded 0.4, its warming effect significantly diminished.

The relationship between FAR and LST exhibited an inverted U-shaped curve, with the inflection point occurring at 1.5. Consistent with our findings, Lin et al. [59] observed a negative correlation between FAR and LST between 3 and 7. Parth Bansal et al. [60] found a positive correlation between FAR and LST between 0.5 and 1.5 and a slight negative correlation between 1.5 and 2. We attributed the formation of this nonlinear relationship to the following reasons: the increase in FAR contributed to the heat storage volume of urban canyons, while also increasing the shading effect on solar radiation [61]. When FAR was less than 1.5, the heat storage effect outweighed the shading effect, resulting in a positive correlation between FAR and LST. However, as the slope gradually flattened, when FAR exceeded 1.5, the shading effect surpassed the heat storage effect, leading to a negative correlation between FAR and LST.

The partial correlation analysis results between BH and LST aligned with the findings of Qi Wang et al. [56]. Within the range of 0–40 m, as BH increased, LST decreased rapidly. Between 40 and 60 m, there was little change in LST with increasing building height. However, when BH exceeded 60 m, LST showed a slight increase with increasing BH. The negative correlation between BH and LST could be explained by the research of Meiya Wang [62]. Meiya Wang revealed a negative logarithmic impact pattern of BH on LST in six major Chinese cities, indicating that as BH increased, LST significantly decreased. This could be attributed to the shading effect of buildings, reducing total solar radiation and effectively lowering urban temperatures. Additionally, there was a clear wind bending or

wind trapping effect in the distribution of buildings, which altered the predominant wind direction around tall buildings, generating turbulence in urban canyons, and creating a 'wind valley' within the local building area. This wind disturbance facilitated the vertical heat transfer, carrying heat near the surface into the air, and ultimately lowering LST. However, this cooling effect had a threshold at 60 m; when the building height exceeded 60 m, the cooling effect brought about by the increase in building height may even transform into a warming effect.

Previous linear analysis studies demonstrated that SVF had a positive impact on LST [12,63,64]. Our nonlinear analysis revealed that SVF demonstrated a positive correlation with LST in the compact classes (LCZ2-3) and the open low-rise class (LCZ6). However, in the open mid-rise class (LCZ5), SVF and LST exhibited a U-shaped relationship, with the inflection point occurring between 0.75 and 0.85. According to Giridharan et al., urban areas with higher SVF had higher LST. On the contrary, Chen et al. found a negative relationship between SVF and LST [65]. Although they admitted that the 'negative' relationship was not clearly addressed, they explained this result through differences in the study area. Therefore, the effect of SVF on LST was still a debatable issue.

SVF served as an indicator of both the surface's capability to receive solar radiation and the cooling capacity of urban canyons [65]. Consequently, as SVF increased, the surface received more solar radiation while also enhancing heat dissipation. The relative strength between these two effects to some extent determined the surface temperature. Hence, the varying correlations between SVF and LST may be attributed to the following reasons: in LCZ2, 3, and 6, when SVF approached 0, the surface received minimal solar radiation, resulting in lower LST. With increasing SVF, although the surface received more solar radiation, the diminishing cooling effect balanced the temperature change. However, when SVF exceeded 0.8 [12], the warming effect due to increased solar radiation outweighed the cooling effect, resulting in a temperature increase and a positive correlation between SVF and LST. In LCZ5, characterized by high human activities such as residential and commercial areas, artificial heat dissipation was significant. When SVF was close to 0, the cooling effect was weak, leading to higher LST compared to other LCZs with the same SVF. As SVF increased, the cooling effect strengthened, resulting in a negative correlation between SVF and LST. Nevertheless, when SVF surpassed 0.8, the surface received substantial solar radiation coupled with significant artificial heat dissipation, leading to a positive correlation between SVF and LST, with LST exceeding that of other LCZs with similar SVF levels.

4.3. Optimization Strategies

The results of nonlinear analysis (as depicted in Figure 8) offer more effective and practical insights for urban planners and managers, aiding cities in enhancing climate adaptability and resilience through precise spatial strategies tailored to different LCZ types.

Firstly, planners should control BD, FAR, and ISF through land use zoning. The concepts of "sponge city", "planning based on natural solutions", and so on should be adopted and carried out. For example, policies such as using facilities like green infrastructures (rain gardens, urban canyon trees, roof top gardening, and the greening of walls), urban parks and permeable pavement instead of concrete [66], and encouraging the use of sustainable urban drainage systems increase permeable surfaces and reduce the proportion of impervious surfaces [23]. In densely built areas, maintaining FAR above 1.5 by coordinating the relationship between building footprint and height can further alleviate the urban heat island effect [67]. Secondly, as for compact class of LCZs, planners could employ "O" or "C" layouts to reduce sky visibility, decreasing the amount of solar radiation received by the ground. This effective mitigation strategy enhances local microclimate comfort and helps alleviate the urban heat island effect [64]. Thirdly, as for open class of LCZs, buildings should adopt "L" or "I" configurations to maximize sky visibility and promote vertical heat turbulence exchange to enlarge the SVF maybe the effective way to decrease the LST, besides BD, FAR, and ISF controlling. Fourthly, BH were not invariable relationship with

LST for each LCZ type. This finding suggests that planners should set a reasonable range of building heights. Government departments should consider incrementally raising building heights within the confines of maintaining the FAR in each LCZ within designated limits, but keep it below 60 m to ensure the best cooling efficiency [62], through regulations such as urban master planning and detailed control planning.

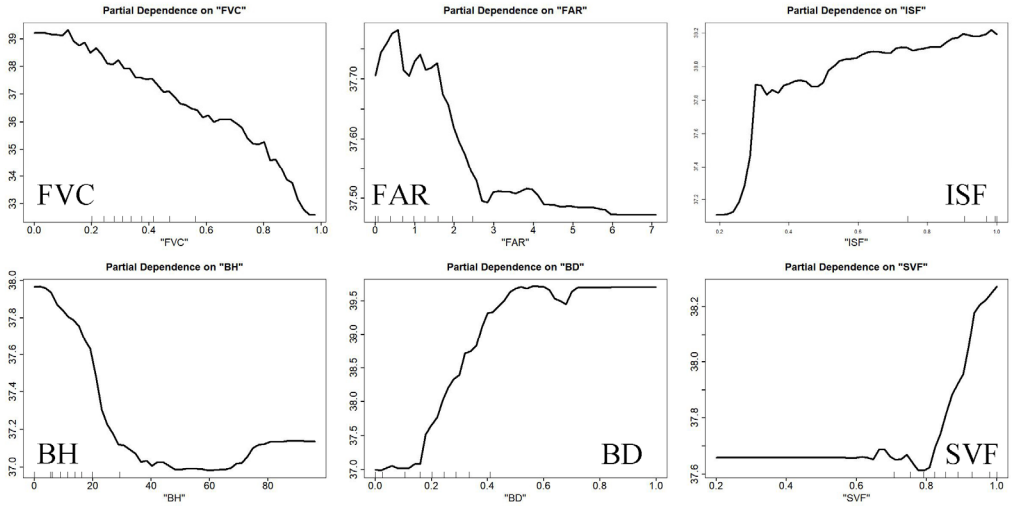

Figure 8. The overall results of the partial correlation analysis.

5. Conclusions

This study employed the Radiation Transfer Equation method to obtain the LST in Xi'an. A GIS-based approach was used to conduct LCZ mapping based on six urban morphology factors. Random forest nonlinear analysis was utilized to investigate the relationship between these urban morphology factors and LST within LCZs.

The findings of this study can be summarized as follows. More than 40% of the study area experienced temperatures exceeding 38 °C, indicating a significant urban heat island effect in Xi'an. FVC contributed the most to the variation in LST, while FAR contributed the least. ISF and BD were found to have a positive impact on LST, while FVC and BH had a negative influence. Moreover, SVF was observed to positively influence LST in the compact classes (LCZ2-3) and open low-rise class (LCZ6). In the open mid-rise class (LCZ5), SVF and LST showed a U-shaped relationship. There is an inverted U-shaped relationship between FAR and LST, with the inflection point occurring at 1.5. The results of nonlinear analysis were beneficial in illustrating the complex relationships between LST and its driving factors. Based on these conclusions, this study proposes strategies to mitigate the urban heat island effect. These strategies include controlling building density and impervious surface fraction within building-class LCZs, while also considering appropriate increases in building height and fractional vegetation coverage. Furthermore, land cover-class LCZs can serve as cool sources, connected by corridors created by rivers, roadways, and green spaces to establish continuous cool zones surrounding building-class LCZs.

However, this research has certain limitations. Firstly, this study mainly focuses on the UHI problem in high-density built-up areas, and whether the relevant conclusions are applicable in rural and suburban areas remains to be confirmed. Secondly, inevitable omissions exist in the selection of urban spatial morphology factors that affect the UHI effect, which will be strengthened in future research.

In conclusion, this study provides a comprehensive analysis of the impact of morphological factors on the urban heat island effect and aims to develop context-specific optimization solutions that align regional climate with socioeconomic development during the urbanization process.

Author Contributions: Conceptualization, C.W., H.Z. and H.Y.; methodology, C.W. and H.Y.; software, Z.M.; validation, H.Z., W.J. and Z.M.; formal analysis, C.W.; investigation, W.J.; resources, C.W.; data curation, H.Z.; writing—original draft preparation, C.W. and W.J.; writing—review and editing, C.W., H.Z. and H.Y.; visualization, Z.M.; supervision, H.Z.; project administration, H.Z. and W.J.; funding acquisition, Z.M. All authors have read and agreed to the published version of the manuscript.

Funding: This research was funded by Shaanxi National Science Foundation, grant number 2021JQ-175, and the Northwest A&F University Student Innovation Program, A Study on the Thermal Environmental Effects of Urban Spatial Form from the Perspective of Local Climate Regions: A Case Study of Yangling District.

Institutional Review Board Statement: Not applicable.

Informed Consent Statement: Not applicable.

Data Availability Statement: Data are contained within the article.

Acknowledgments: The authors are grateful to the reviewers for their constructive comments.

Conflicts of Interest: The authors declare no conflicts of interest.

Abbreviations

LST	Land Surface Temperature
UHI	Urban Heat Island
UHII	Urban Heat Island Intensity
LCZ	Local Climate Zone
BD	Building Density
FAR	Floor Area Ratio
SVF	Sky View Factor
ISF	Impervious Surface Fraction
WR	Water Ratio
FVC	Fractional Vegetation Coverage
BH	Average Building Height
RTE	Radiative Transfer Equation

References

1. Arnfield, A.J. Two decades of urban climate research: A review of turbulence, exchanges of energy and water, and the urban heat island. *Int. J. Climatol. A J. R. Meteorol. Soc.* **2003**, *23*, 1–26. [CrossRef]
2. Laurent, J.G.C.; Williams, A.; Oulhote, Y.; Zanobetti, A.; Allen, J.G.; Spengler, J.D. Reduced cognitive function during a heat wave among residents of non-air-conditioned buildings: An observational study of young adults in the summer of 2016. *PLoS Med.* **2018**, *15*, e1002605.
3. Vicedo-Cabrera, A.M.; Scovronick, N.; Sera, F.; Royé, D.; Schneider, R.; Tobias, A.; Astrom, C.; Guo, Y.; Honda, Y.; Hondula, D. The burden of heat-related mortality attributable to recent human-induced climate change. *Nat. Clim. Change* **2021**, *11*, 492–500. [CrossRef]
4. Santamouris, M. Recent progress on urban overheating and heat island research. Integrated assessment of the energy, environmental, vulnerability and health impact. Synergies with the global climate change. *Energy Build.* **2020**, *207*, 109482. [CrossRef]
5. Nasehi, S.; Yavari, A.; Salehi, E.; Emmanuel, R. Role of local climate zone and space syntax on land surface temperature (case study: Tehran). *Urban Clim.* **2022**, *45*, 101245. [CrossRef]
6. Abdullah, S.; Barua, D. modeling land surface temperature with a mono-window algorithm to estimate urban heat Island intensity in an expanding Urban Area. *Environ. Process.* **2022**, *9*, 14. [CrossRef]
7. Ali, S.A.; Parvin, F.; Ahmad, A. Retrieval of land surface temperature from Landsat 8 OLI and TIRS: A comparative analysis between radiative transfer equation-based method and split-window algorithm. *Remote Sens. Earth Syst. Sci.* **2023**, *6*, 1–21. [CrossRef]
8. Dejun, Z.; Shiqi, Y.; Liang, S.; Xiaoran, L.; Shihao, T.; Hao, Z.; Qinyu, Y.; Xinyu, Z. Retrieval of land surface temperature from FY3D MERSI-II based on re-fitting Split Window Algorithm. *Eur. J. Remote Sens.* **2022**, *55*, 1–18. [CrossRef]
9. Yu, X.; Guo, X.; Wu, Z. Land surface temperature retrieval from Landsat 8 TIRS—Comparison between radiative transfer equation-based method, split window algorithm and single channel method. *Remote Sens.* **2014**, *6*, 9829–9852. [CrossRef]

10. Nasar-u-Minallah, M.; Haase, D.; Qureshi, S.; Zia, S.; Fatima, M. Ecological monitoring of urban thermal field variance index and determining the surface urban heat island effects in Lahore, Pakistan. *Environ. Monit. Assess.* **2023**, *195*, 1212. [CrossRef]
11. Kim, S.W.; Brown, R.D. Urban heat island (UHI) variations within a city boundary: A systematic literature review. *Renew. Sustain. Energy Rev.* **2021**, *148*, 111256. [CrossRef]
12. Guo, G.H.; Zhou, X.Q.; Wu, Z.F.; Xiao, R.B.; Chen, Y.B. Characterizing the impact of urban morphology heterogeneity on land surface temperature in Guangzhou, China. *Environ. Model. Softw.* **2016**, *84*, 427–439. [CrossRef]
13. Dirksen, M.; Ronda, R.; Theeuwes, N.; Pagani, G. Sky view factor calculations and its application in urban heat island studies. *Urban Clim.* **2019**, *30*, 100498. [CrossRef]
14. Qi, Y.; Li, H.; Pang, Z.; Gao, W.; Liu, C. A case study of the relationship between vegetation coverage and urban heat island in a coastal city by applying digital twins. *Front. Plant Sci.* **2022**, *13*, 861768. [CrossRef]
15. Zhang, P.; Ghosh, D.; Park, S. Spatial measures and methods in sustainable urban morphology: A systematic review. *Landsc. Urban Plan.* **2023**, *237*, 104776. [CrossRef]
16. Duckworth, F.S.; Sandberg, J.S. The effect of cities upon horizontal and vertical temperature gradients. *Bull. Am. Meteorol. Soc.* **1954**, *35*, 198–207. [CrossRef]
17. Stewart, I.D.; Oke, T.R.; Krayenhoff, E.S. Evaluation of the 'local climate zone'scheme using temperature observations and model simulations. *Int. J. Climatol.* **2014**, *34*, 1062–1080. [CrossRef]
18. Stewart, I.D.; Oke, T.R. Local Climate Zones for Urban Temperature Studies. *Bull. Am. Meteorol. Soc.* **2012**, *93*, 1879–1900. [CrossRef]
19. Zhao, Z.Q.; Sharifi, A.; Dong, X.; Shen, L.D.; He, B.J. Spatial Variability and Temporal Heterogeneity of Surface Urban Heat Island Patterns and the Suitability of Local Climate Zones for Land Surface Temperature Characterization. *Remote Sens.* **2021**, *13*, 4338. [CrossRef]
20. Xu, Y.N.; Zhang, C.X.; Hou, W. Modeling of Daytime and Nighttime Surface Urban Heat Island Distribution Combined with LCZ in Beijing, China. *Land* **2022**, *11*, 2050. [CrossRef]
21. Wang, Z.; Ishida, Y.; Mochida, A. Effective Factors for Reducing Land Surface Temperature in Each Local Climate Zone Built Type in Tokyo and Shanghai. *Remote Sens.* **2023**, *15*, 3840. [CrossRef]
22. Zhang, Q.; Xu, D.; Zhou, D.; Yang, Y.J.; Rogora, A. Associations between urban thermal environment and physical indicators based on meteorological data in Foshan City. *Sustain. Cities Soc.* **2020**, *60*, 10. [CrossRef]
23. Estoque, R.C.; Murayama, Y.; Myint, S.W. Effects of landscape composition and pattern on land surface temperature: An urban heat island study in the megacities of Southeast Asia. *Sci. Total Environ.* **2017**, *577*, 349–359. [CrossRef] [PubMed]
24. Gao, Y.J.; Zhao, J.Y.; Han, L. Exploring the spatial heterogeneity of urban heat island effect and its relationship to block morphology with the geographically weighted regression model. *Sustain. Cities Soc.* **2022**, *76*, 13. [CrossRef]
25. Rigatti, S.J. Random Forest. *J. Insur. Med.* **2017**, *47*, 31–39. [CrossRef] [PubMed]
26. Ming, Y.J.; Liu, Y.; Gu, J.P.; Wang, J.Z.; Liu, X. Nonlinear effects of urban and industrial forms on surface urban heat island: Evidence from 162 Chinese prefecture-level cities. *Sustain. Cities Soc.* **2023**, *89*, 14. [CrossRef]
27. Gao, Y.J.; Zhao, J.Y.; Han, L. Quantifying the nonlinear relationship between block morphology and the surrounding thermal environment using random forest method. *Sustain. Cities Soc.* **2023**, *91*, 16. [CrossRef]
28. Yang, C.; Kui, T.; Zhou, W.; Fan, J.; Pan, L.; Wu, W.; Liu, M. Impact of refined 2D/3D urban morphology on hourly air temperature across different spatial scales in a snow climate city. *Urban Clim.* **2023**, *47*, 101404. [CrossRef]
29. Oke, T.R. Canyon geometry and the nocturnal urban heat island: Comparison of scale model and field observations. *J. Climatol.* **1981**, *1*, 237–254. [CrossRef]
30. Geletič, J.; Lehnert, M. GIS-based delineation of local climate zones: The case of medium-sized Central European cities. *Morav. Geogr. Rep.* **2016**, *24*, 2–12. [CrossRef]
31. Geletic, J.; Lehnert, M.; Dobrovolny, P. Land Surface Temperature Differences within Local Climate Zones, Based on Two Central European Cities. *Remote Sens.* **2016**, *8*, 788. [CrossRef]
32. Shi, Y.; Xiang, Y.; Zhang, Y. Urban design factors influencing surface urban heat island in the high-density city of Guangzhou based on the local climate zone. *Sensors* **2019**, *19*, 3459. [CrossRef]
33. Yuan, B.; Zhou, L.; Hu, F.; Zhang, Q. Diurnal dynamics of heat exposure in Xi'an: A perspective from local climate zone. *Build. Environ.* **2022**, *222*, 109400. [CrossRef]
34. Li, F.; Chen, W.; Zeng, Y.; Zhao, Q.; Wu, B. Improving estimates of grassland fractional vegetation cover based on a pixel dichotomy model: A case study in Inner Mongolia, China. *Remote Sens.* **2014**, *6*, 4705–4722. [CrossRef]
35. O'Malley, C.; Kikumoto, H. An investigation into heat storage by adopting local climate zones and nocturnal-diurnal urban heat island differences in the Tokyo Prefecture. *Sustain. Cities Soc.* **2022**, *83*, 103959. [CrossRef]
36. Cui, S.Y.; Wang, X.H.; Yang, X.; Hu, L.F.; Jiang, Z.Q.; Feng, Z.H. Mapping Local Climate Zones in the Urban Environment: The Optimal Combination of Data Source and Classifier. *Sensors* **2022**, *22*, 6407. [CrossRef] [PubMed]
37. Zhao, C.H.; Jensen, J.L.R.; Weng, Q.H.; Currit, N.; Weaver, R. Use of Local Climate Zones to investigate surface urban heat islands in Texas. *GIScience Remote Sens.* **2020**, *57*, 1083–1101. [CrossRef]
38. Du, P.J.; Chen, J.K.; Bai, X.Y.; Han, W.Q. Understanding the seasonal variations of land surface temperature in Nanjing urban area based on local climate zone. *Urban Clim.* **2020**, *33*, 100657. [CrossRef]

39. Fang, T.Y.; Mu, K.; Liu, Y.; Zhang, M.; Han, B.; Yang, L.; Khaletski, V. Investigations of Surface Urban Heat Island Effect Based on Local Climate Zone Method: A Case of Xi'an. *E3S Web Conf.* **2019**, *136*, 05011. [CrossRef]
40. Shi, L.F.; Ling, F.; Foody, G.M.; Yang, Z.; Liu, X.X.; Du, Y. Seasonal SUHI Analysis Using Local Climate Zone Classification: A Case Study of Wuhan, China. *Int. J. Environ. Res. Public Health* **2021**, *18*, 7242. [CrossRef]
41. Zhang, L.P.; Zhou, L.; Yuan, B.; Hu, F.N.; Zhang, Q.; Wei, W.; Sun, D.Q. Spatiotemporal Evolution Characteristics of Urban Land Surface Temperature Based on Local Climate Zones in Xi'an Metropolitan, China. *Chin. Geogr. Sci.* **2023**, *33*, 1001–1016. [CrossRef]
42. Yang, X.Y.; Li, Y.G.; Luo, Z.W.; Chan, P.W. The urban cool island phenomenon in a high-rise high-density city and its mechanisms. *Int. J. Climatol.* **2017**, *37*, 890–904. [CrossRef]
43. Cai, M.; Ren, C.; Xu, Y.; Lau, K.K.L.; Wang, R. Investigating the relationship between local climate zone and land surface temperature using an improved WUDAPT methodology—A case study of Yangtze River Delta, China. *Urban Clim.* **2018**, *24*, 485–502. [CrossRef]
44. Yang, X.S.; Yao, L.Y.; Jin, T.; Peng, L.L.H.; Jiang, Z.D.; Hu, Z.Y.; Ye, Y.H. Assessing the thermal behavior of different local climate zones in the Nanjing metropolis, China. *Build. Environ.* **2018**, *137*, 171–184. [CrossRef]
45. Liu, Y.; Li, Q.; Yang, L.; Mu, K.K.; Zhang, M.Y.; Liu, J.P. Urban heat island effects of various urban morphologies under regional climate conditions. *Sci. Total Environ.* **2020**, *743*, 140589. [CrossRef] [PubMed]
46. He, B.J.; Ding, L.; Prasad, D. Relationships among local-scale urban morphology, urban ventilation, urban heat island and outdoor thermal comfort under sea breeze influence. *Sustain. Cities Soc.* **2020**, *60*, 102289. [CrossRef]
47. Zhou, L.; Yuan, B.; Hu, F.; Wei, C.; Dang, X.; Sun, D. Understanding the effects of 2D/3D urban morphology on land surface temperature based on local climate zones. *Build. Environ.* **2022**, *208*, 108578. [CrossRef]
48. Ferreira, L.S.; Duarte, D.H.S. Exploring the relationship between urban form, land surface temperature and vegetation indices in a subtropical megacity. *Urban Clim.* **2019**, *27*, 105–123. [CrossRef]
49. Lin, Z.; Xu, H.; Yao, X.; Yang, C.; Yang, L. Exploring the relationship between thermal environmental factors and land surface temperature of a "furnace city" based on local climate zones. *Build. Environ.* **2023**, *243*, 110732. [CrossRef]
50. Moss, J.L.; Doick, K.J.; Smith, S.; Shahrestani, M. Influence of evaporative cooling by urban forests on cooling demand in cities. *Urban For. Urban Green.* **2019**, *37*, 65–73. [CrossRef]
51. Zhang, Y.; Odeh, I.O.; Ramadan, E. Assessment of land surface temperature in relation to landscape metrics and fractional vegetation cover in an urban/peri-urban region using Landsat data. *Int. J. Remote Sens.* **2013**, *34*, 168–189. [CrossRef]
52. Zheng, B.; Myint, S.W.; Fan, C. Spatial configuration of anthropogenic land cover impacts on urban warming. *Landsc. Urban Plan.* **2014**, *130*, 104–111. [CrossRef]
53. Alavipanah, S.; Wegmann, M.; Qureshi, S.; Weng, Q.; Koellner, T. The role of vegetation in mitigating urban land surface temperatures: A case study of Munich, Germany during the warm season. *Sustainability* **2015**, *7*, 4689–4706. [CrossRef]
54. Akbari, H.; Pomerantz, M.; Taha, H. Cool surfaces and shade trees to reduce energy use and improve air quality in urban areas. *Sol. Energy* **2001**, *70*, 295–310. [CrossRef]
55. Voogt, J.A.; Oke, T.R. Thermal remote sensing of urban climates. *Remote Sens. Environ.* **2003**, *86*, 370–384. [CrossRef]
56. Wang, Q.; Wang, X.N.; Zhou, Y.; Liu, D.Y.; Wang, H.T. The dominant factors and influence of urban characteristics on land surface temperature using random forest algorithm. *Sustain. Cities Soc.* **2022**, *79*, 18. [CrossRef]
57. Chen, Y.-C.; Lin, T.-P.; Lin, C.-T. A simple approach for the development of urban climatic maps based on the urban characteristics in Tainan, Taiwan. *Int. J. Biometeorol.* **2017**, *61*, 1029–1041. [CrossRef] [PubMed]
58. Goward, S.N. Thermal behavior of urban landscapes and the urban heat island. *Phys. Geogr.* **1981**, *2*, 19–33. [CrossRef]
59. Lin, P.Y.; Lau, S.S.Y.; Qin, H.; Gou, Z.H. Effects of urban planning indicators on urban heat island: A case study of pocket parks in high-rise high-density environment. *Landsc. Urban Plan.* **2017**, *168*, 48–60. [CrossRef]
60. Bansal, P.; Quan, S.J. Examining temporally varying nonlinear effects of urban form on urban heat island using explainable machine learning: A case of Seoul. *Build. Environ.* **2024**, *247*, 20. [CrossRef]
61. Huang, H.C.; Yun, Y.X.; Xu, J.G.; Huang, R.; Fu, J.; Huang, K.D. Scale Response of Summer Urban Heat Island to Building Plot Ratio and Its Warning Parameter. *Teh. Vjesn.* **2017**, *24*, 877–886. [CrossRef]
62. Wang, M.; Xu, H. The impact of building height on urban thermal environment in summer: A case study of Chinese megacities. *PLoS ONE* **2021**, *16*, e0247786. [CrossRef] [PubMed]
63. Giridharan, R.; Lau, S.S.Y.; Ganesan, S.; Givoni, B. Lowering the outdoor temperature in high-rise high-density residential developments of coastal Hong Kong: The vegetation influence. *Build. Environ.* **2008**, *43*, 1583–1595. [CrossRef]
64. Kim, J.; Lee, D.-K.; Brown, R.D.; Kim, S.; Kim, J.-H.; Sung, S. The effect of extremely low sky view factor on land surface temperatures in urban residential areas. *Sustain. Cities Soc.* **2022**, *80*, 103799. [CrossRef]
65. Chen, L.; Ng, E.; An, X.P.; Ren, C.; Lee, M.; Wang, U.; He, Z.J. Sky view factor analysis of street canyons and its implications for daytime intra-urban air temperature differentials in high-rise, high-density urban areas of Hong Kong: A GIS-based simulation approach. *Int. J. Climatol.* **2012**, *32*, 121–136. [CrossRef]

66. Zhou, S.Y.; Zheng, H.; Liu, X.; Gao, Q.; Xie, J. Identifying the Effects of Vegetation on Urban Surface Temperatures Based on Urban-Rural Local Climate Zones in a Subtropical Metropolis. *Remote Sens.* **2023**, *15*, 4743. [CrossRef]
67. Luo, P.Y.; Yu, B.J.; Li, P.F.; Liang, P.P.; Zhang, Q.Y.; Yang, L.C. Understanding the relationship between 2D/3D variables and land surface temperature in plain and mountainous cities: Relative importance and interaction effects. *Build. Environ.* **2023**, *245*, 110959. [CrossRef]